Chemical Geology 554 (2020) 119800

Contents lists available at ScienceDirect

Chemical Geology

journal homepage: www.elsevier.com/locate/chemgeo

An assessment of iron isotope fractionation during core formation

Anat Shahar[a,*], Edward D. Young[b]

[a] Earth and Planets Laboratory, Carnegie Institution for Science, United States of America
[b] Department of Earth, Planetary, and Space Sciences, UCLA, United States of America

ARTICLE INFO

Editor: Catherine Chauvel

Keywords:
Core formation
Iron isotopes
High-temperature experiments
Equilibrium isotope fractionation

ABSTRACT

Iron is a ubiquitous element in terrestrial and extra-terrestrial settings and can provide clues as to the conditions during which planetary scale processes occurred. One example of this is determining the conditions accompanying metal core formation in rocky planets and planetesimals. For at least two decades there has been a growing database of experimental and natural data aimed at understanding whether iron isotopes fractionate during the separation of silicate and metal. While it has been argued that the data are not in agreement with one another, it is apparent that once criteria are established that prove equilibrated samples, there is good agreement amongst the different studies when looked at as a function of the metallic composition. Proving equilibrium is critical in these types of experiments. The three-isotope experimental technique for establishing equilibrium is found to be both mathematically and fundamentally sound. Further it is clear that the question of whether there is an equilibrium iron isotope fractionation between metal and silicate is not straightforward and that it can vary significantly as a function of temperature, pressure, metallic composition, oxygen fugacity, and silicate composition.

1. Introduction

A series of papers were published starting in 1999 that showed that iron isotope variations in terrestrial samples could sometimes be attributed to biological processes (Beard et al., 1999; Beard and Johnson, 1999; Mandernack et al., 1999). The two studies from the University of Wisconsin showed for the first time with high precision that most terrestrial and lunar high temperature samples have δ^{56}Fe values (^{56}Fe/^{54}Fe relative to a terrestrial standard in per mil) near 0‰ while rocks that had been produced by biological activity such as Fe–Mn nodules, banded iron formations, as well as experiments with microorganisms, showed a large range in δ^{56}Fe values of ~2‰. These papers suggested that iron isotopes could be used as tracers for biologic activity, possibly even going back in time. It soon became clear however, that abiotic processes in aqueous systems could also fractionate iron isotopes and hence the tracing of biologic activity through the use of iron isotopes became more difficult (e.g. Bullen et al., 2001; Schauble et al., 2001). Over the next few years as MC-ICPMS (multiple-collector inductively coupled plasma source mass spectrometer) techniques developed and improved, the precision with which analyses were made increased significantly while at the same time, hundreds, if not thousands, of measurements were made on natural terrestrial and extra-terrestrial samples (e.g. Zhu et al., 2002; Weyer and Schwieters, 2003; Beard et al., 2003). The aim was to determine whether iron isotope fractionation could be used as a tracer of processes where other more traditional stable isotopes could not be used. As iron is a major element, ubiquitous, and a multivalent transition metal, its isotopes could be powerful tracers of geochemical processes, including planetary differentiation.

Several reviews have already been written about iron stable isotope geochemistry as a whole (e.g. Beard and Johnson, 2004; Dauphas et al., 2018). In this paper we focus on understanding whether iron isotopes can be used as a tracer of high-temperature planetary scale processes, and in particular, planetary differentiation. There are several ways to test whether planetary scale processes can fractionate iron isotopes, including conducting experiments, analyzing terrestrial mantle rocks such as peridotites, analyzing samples from differentiated meteorites representing planetary bodies such as the Moon, Mars and Vesta, as well as unknown parent bodies, and calculating fractionation factors amongst phases at high temperatures. Starting in 2004, a series of papers did just this and a controversy erupted as to whether or not iron isotopes are fractionated during planetary differentiation.

The first and most fundamental problem has been inferring the iron isotopic composition of the bulk Earth. Initial iron isotope work on natural samples determined that 'Earth' (meaning mantle-derived rocks) was ~0.1‰ higher in ^{57}Fe/^{54}Fe than rocks from Mars and Vesta

* Corresponding author.
E-mail address: ashahar@carnegiescience.edu (A. Shahar).

https://doi.org/10.1016/j.chemgeo.2020.119800
Received 24 March 2020; Received in revised form 2 July 2020; Accepted 27 July 2020
Available online 02 August 2020
0009-2541/

and that lunar basalts were ~0.1‰ higher than the Earth's mantle (Poitrasson et al., 2004). The authors hypothesized that these differences were due to partial vaporization, which led to a kinetic iron isotope fractionation (consistent with the Moon-forming giant impact). As Earth and the Moon were calculated to be in excess of 3000 K and largely molten, the light iron isotopes, it was thought, would have evaporated preferentially, leaving behind a residue with high $^{57}Fe/^{54}Fe$. Soon thereafter, iron meteorites were found to be systematically isotopically heavy compared with chondritic iron isotope ratios and pallasitic metals were found to be more enriched in heavy iron isotopes than pallasite olivines (Poitrasson et al., 2005). Due to the lack of fractionation of Fe isotopes found amongst planetary materials earlier (Mars, Vesta, Earth), it was concluded that these variations were not due to planetary differentiation, but instead the result of local processes and/or accretion mechanisms as well as sample bias. In 2005, Weyer et al., suggested that there was in fact an iron isotope fractionation during planetary differentiation based on analyzing a new suite of planetary materials from Mars, Vesta, pallasites, and Earth's mantle. The evidence for and against isotope fractionation during core formation relies critically on knowing what the bulk Earth iron isotope value is. There continues to be disagreement about this value and therefore no way to know whether other objects are fractionated relative to Earth, or to chondrite.

In 2009 Polyakov predicted that core-mantle differentiation would leave an imprint on the iron isotope signature of the Bulk Silicate Earth due to the valence state difference of Fe between lower-mantle Fe^{2+} and Fe^{3+} bearing minerals and Fe^0 metal at the core-mantle-boundary. He suggested that the enrichment of Earth/Moon basalts in heavy iron isotopes relative to those from Mars/Vesta is due to equilibrium iron isotope fractionation during Earth's core formation. His calculations (based on high pressure ^{57}Fe partial vibrational density of states) show that pressure has a significant impact on the isotopic fractionation factor between mantle minerals and iron metal, and the direction of the fractionation changes as the minerals move from ambient conditions to core mantle boundary conditions. Williams et al. (2012) suggested that disproportionation of Fe^{2+} in silicates at high pressure to Fe^0 and Fe^{3+} (into silicate perovskite) was a means to explain the non-chondritic terrestrial mantle. However, Craddock et al. (2013) added more data and models to an alternative explanation that had been proposed earlier (Dauphas et al., 2009; Weyer and Ionov, 2007; Williams et al., 2004) arguing that the bulk silicate Earth was chondritic and that it was the terrestrial basalts that were not chondritic. The model suggests there might be an iron isotopic fractionation during partial melting. Therefore, there were three main hypotheses regarding the iron isotopic composition of the Earth – that the heavy isotopic signature in basalts was due to partial melting in the mantle, that the heavy signature in basalts was due to core formation, or that the bulk Earth was heavy relative to chondrite due to vaporization as a result of the giant impact.

Since then there has not been a consensus on the iron isotopic signature of the bulk Earth (e.g. Sossi et al., 2016) or if the three processes outlined above are responsible for any high temperature iron isotopic fractionation seen on Earth today. In this paper we focus on whether iron isotopes can be fractionated during core formation on Earth by examining all the data published to date on the topic. Both volatilization (e.g. Sossi et al., 2016; Jordan et al., 2019) and partial melting/magma differentiation (e.g. Dauphas et al., 2014; Sossi et al., 2012) are still considered plausible mechanisms for causing an iron isotope fractionation at high temperature and it is likely that several processes are at play in creating what is now a heterogeneous mantle with respect to iron isotopes.

As the Earth grew to its present size, it separated into several layers in a multi-stage fashion with the denser liquid iron moving towards the center of the planet. It is assumed in experimental isotope studies that the metal and silicate fully equilibrated prior to separating into layers to first order. While this is likely not the case, it is simplest to assume at this point as it is not possible to simulate inefficient core formation during an experiment. Therefore, it is important to determine if there is an equilibrium stable isotope fractionation between metal and silicate. To first order it is important to determine if there is a resolvable fractionation at any conditions, and then to proceed by understanding how that fractionation could change as a function of pressure, temperature, and composition. The temperature and pressure associated with core formation on Earth has been estimated from modeling accretion as well as trying to fit siderophile element concentrations in the mantle (e.g Badro et al., 2015; Rubie et al., 2015). While core formation is generally considered to be a multi-stage process that occurred over a range of pressures and temperatures, the average value is approximately 40–60 GPa and 3500 K (e.g. Corgne et al., 2009). The composition of the mantle is thought to be that of pyrolite, whereas the composition of the core is much more uncertain. On Earth, seismic data show the density difference between pure iron and the apparent density of the core. This discrepancy implies that there are 'light' elements other than iron within the core of the Earth (Birch, 1964). As the molten iron metal moved to the center of the planetary body it picked up other elements and formed an impure iron-nickel rich alloy. It is thought that this is the case on other planetary bodies as well. The elements the iron bonds with are a function of the conditions associated with core formation. For example, at high temperature under reducing conditions, silicon is likely to alloy with iron, however, under more oxidizing conditions oxygen is likely to enter the metal (Badro et al., 2015). Determining whether there is an equilibrium iron isotope fractionation between metal and silicate will need to take into account all of these variables.

2. Experimental Methods

2.1. Experimental methods to constrain isotope fractionation

A thorough explanation of the various experimental methods and their advantages and disadvantages can be found in a review by Shahar et al. (2017). In this paper, we quickly review the two main techniques used for constraining core formation using iron isotope fractionation: piston cylinder experiments and Nuclear Resonant Inelastic X-ray Scattering (NRIXS). A piston cylinder apparatus is a common instrument in an experimental petrology laboratory (Boyd and England, 1960). The advantage of such a press is that the material is sealed in a capsule, allowing for a closed system throughout the experiment with respect to the element of choice, allowing for equilibrium to be attained more easily. Most experiments are carried out using a ½-inch piston-cylinder cell assembly, typically maintaining a pressure of 1–2 GPa at temperatures up to ~1800C. The choice of capsule material is crucial to the success of the experiment; in order to assess the approach to isotopic equilibrium and ensure that the possibility of kinetic processes is limited, a closed system must be maintained. An open system, with respect to isotope exchange, will in all likelihood result in non-equilibrium conditions during the experiment. Therefore, a capsule that alloys or reacts with the element of interest should not be used for the experiment. This excludes the use of metal capsules in metal-silicate experiments simulating core formation. Experience shows that metal capsules often result in a loss of the element of interest into the capsule or the creation of a mineral on the capsule wall that has an isotope fractionation that can be limited by kinetics (e.g., diffusion), thereby limiting the opportunity for equilibrium isotope exchange amongst the phases of interest. Experiments in the piston cylinder have relied on a time series approach or utilized the three-isotope technique to address isotopic equilibrium (discussed in much more detail below). The beauty of these experiments is that the two phases of interest are in the capsule and experiencing the same conditions. Further, at the end of the experiment, the phases are separated, purified, and then analyzed with the MC-ICPMS. There are no calculations that are needed to determine the fractionation between the two phases. The values are immediately obtained from the mass spectrometer. In recent years, a new technique, NRIXS, has allowed the determination of iron isotope fractionation

using reduced partition function ratios, or beta factors, at high pressure. The method in essence provides the means to estimate the effects of isotope substitution on vibrational partition functions that control isotope fractionation between phases.

Therefore, in one case, we have direct experiments where we equilibrate the phases of interest (metal and silicate), and analyze the actual chemical and isotopic exchange occurring between them, at high P and T in the lab, mimicking what happens in nature. In the other case we assess the physical bonding properties (force constants) of the chemical species of interest in each of the phases (metal and silicate) separately, and link those force constants to isotopic fractionation. No isotopes are ever exchanged here, as there is no phase equilibrium involved, since these are single-phase experiments. These radically different approaches have each clear advantages and shortcomings, which will be discussed in the text below. A clear advantage of phase equilibration experiments is the direct measurement of the isotopic compositions, and linking them to an actual fractionation. Once equilibrium is attained, the work is done. The NRIXS technique only interrogates the bonds that are changing, which is the underlying physics behind isotope fractionation, but requires additional steps in modeling. The advantage of NRIXS on the other hand is that it has no pressure limitations, and in principle no temperature limitation either, whereas phase equilibration is limited in pressure and temperatures achievable in the piston cylinder and multi-anvil presses. Also NRIXS doesn't require stringent tests of attainment of isotopic equilibrium, since no isotopes are ever exchanged.

2.2. NRIXS experiments

The basis of the NRIXS method is as follows. The probability for the occurrence of a vibrational energy level corresponding to quantum number n and frequency ν_i, $P(E(n, \nu_i))$, as a function of temperature is calculable from the Boltzmann factor for that energy level:

$$P(E(n,\nu_i)) = \exp\left(-\frac{\left(n+\frac{1}{2}\right)h\nu_i}{k_b T}\right) \tag{1}$$

where k_b is the Boltzmann constant and h is the Planck constant. Eq. (1) can be rewritten using the substitution

$$u_i = \frac{h\nu_i}{k_b T} \tag{2}$$

to obtain

$$P(E(n,u_i)) = e^{-\left(n+\frac{1}{2}\right)u_i} \tag{3}$$

Because the probabilities in Eq. (3) are exclusive, the total probability for all n, $P_{\nu i}$, is the sum of the Boltzmann factors over all n, and this sum can be evaluated as a geometric series:

$$P_{\nu_i} = \sum_{n=0}^{n=\infty} (e^{-u_i})^{\left(n+\frac{1}{2}\right)} = \frac{(e^{-u_i})^{1/2} - (e^{-u_i})^{\infty}}{1-e^{-u_i}} = \frac{e^{-u_i/2}}{1-e^{-u_i}} \tag{4}$$

The total probability for all vibrational frequencies occurring *simultaneously* is the product of probabilities for a single frequency given by Eq. (4). This product is referred to as the vibrational partition function Q_{vib}:

$$Q_{\text{vib}} = \prod_i \frac{e^{-u_i/2}}{1-e^{-u_i}} \tag{5}$$

Eq. (5) can be evaluated more generally by taking the logarithm and replacing the resulting sum over vibrational frequencies with an integral that weights each term by the density of vibrational states $g(\nu_i)$, or the number of modes per unit frequency, yielding

$$\ln Q_{\text{vib}} = \int_0^{\nu_{i,\max}} \ln\left(\frac{e^{-u_i/2}}{1-e^{-u_i}}\right) g(\nu_i)\,d\nu_i$$
$$= \int_0^{\nu_{i,\max}} \left[-\frac{u_i}{2} - \ln(1-e^{-u_i})\right] g(\nu_i)\,d\nu_i \tag{6}$$

Eq. (6) shows that the shape of $g(\nu_i)$ (the density of states, DOS) defines the vibrational partition function. This is the basis for extracting isotope fractionation factors from measurements of densities of state using NRIXS (e.g., Murphy et al., 2013). From the vibrational partition functions one obtains the reduced partition function ratio:

$$\beta = \frac{Q'_{\text{vib}}}{Q_{\text{vib}}}\left(\frac{m}{m'}\right)^{3/2} \tag{7}$$

where the prime symbol refers to the heavy isotope. Ratios of reduced partition function ratios yield fractionation factors between phases. For phases x and y, for example, the fractionation factor $\alpha_{x\text{-}y}$ is

$$\alpha_{x\text{-}y} = \frac{\beta_x}{\beta_y} \tag{8}$$

more commonly expressed as $\ln(\alpha_{x\text{-}y}) = \ln\beta_x - \ln\beta_y$ since $10^3 \ln(\alpha_{x\text{-}y}^{57/54}) \sim \delta^{57}\text{Fe}_x - \delta^{57}\text{Fe}_y = \Delta^{57}\text{Fe}_{x\text{-}y}$ and the differences in isotope ratios are expressed as differences in delta values for most applications. In the NRIXS method, the density of states required to evaluate Eq. (6), and thus eventually Eq. (8), is obtained from the x-ray scattering energy spectrum for the phase of interest.

The partial phonon density of states (PDOS), the contribution to the DOS by the atom of interest (e.g., Fe), can be expressed as an average force constant. Consider the force constant F for a single angular frequency ω of an oscillator: $F = m\,\omega^2$. Since the energy of the oscillation is given by $E = \hbar\omega$ where $\hbar$ is h/(2π), we have

$$F = m\frac{E^2}{\hbar^2} \tag{9}$$

The weighted average force constant is obtained from the PDOS, this time expressed in terms of energy to be consistent with the form of the NRIXS data (g(E) with units of 1/eV and where $\int g(E)dE = 1$), yielding

$$\langle F \rangle = \frac{m}{\hbar^2}\int_0^{E_{\max}} E^2 g(E)\,dE \tag{10}$$

In practice, the scattered x-ray intensity versus energy data obtained using NRIXS are used to obtain average force constants for Fe from either the PDOS as above or from the higher-order moments of the phonon excitation probability density itself, $S(E)$, the normalized primary data for inelastic scattering. The data are thus commonly processed using one of two data reduction software methods – SciPhon (Dauphas et al., 2018) and/or PHOENIX (Sturhahn et al., 1995). Both methods provide an average force constant for the Fe atoms within the phase being probed. However, the methods do not calculate these force constants in the same way and do not always give the same results. PHOENIX analyzes the data obtained by NRIXS and exports three different force constants. The first is the determination of the force constant using the moments approach in which the normalized excitation probability is computed using the raw data and the experimental resolution function. The outcome is based on the raw data and therefore multiphonon contributions are included in the analysis. The second determination of the force constant is also based on this moments approach however it is based on data that is first 'refined', that is, the multiphonon contribution is corrected for and $S(E)$ is extrapolated to higher energies. Dauphas et al. (2012) argue that this moments approach is the best method for determining the force constant as it has smaller uncertainties, is not as dependent on the background and it not as sensitive to asymmetric scans. The third determination of the force constant is based on the partial density of states that is computed from the raw data. The force constant calculated from the PDOS is therefore only based on the one phonon contribution of the data and does not

need to be corrected for the possible multiple phonon contributions. Murphy et al. (2013) suggest that this last force constant calculation is best for determining the force constants. Dauphas et al. (2012) disagree and therefore introduced SciPhon (Dauphas et al., 2018), which calculates force constants directly from the spectra taking into account the backgrounds and errors inherent within. They argue that longer acquisition times are necessary to determine the PDOS of the phases at high pressure with particular emphasis on the high energy tail. Whenever possible both methods should be used until they agree, providing greater confidence in the derived force constant.

Once the force constant, F, is known, it can be used to define the reduced partition function ratio β (Murphy et al., 2013; Dauphas et al., 2012):

$$\ln\beta = \left(\frac{1}{m'} - \frac{1}{m}\right)\frac{\hbar^2}{8k_b^2T^2}\langle F\rangle \tag{11}$$

and the beta factors for two phases can be combined to define the fractionation factor.

Because it characterizes the bonding in a single phase, the NRIXS method avoids some of the pitfalls of piston cylinder experiments. There is no need to prove equilibrium between phases during the experiment and there are no capsules that could interact with the sample. However, this technique requires that the samples be in the solid state which is not ideal when trying to understand processes such as core formation that are thought to occur amongst molten phases. It has been argued (e.g. Shahar et al., 2016; Liu et al., 2017) that Fe isotope fractionation between solids and melts of the same composition should be small if not negligible and that the beta factors derived for solids (glasses) with NRIXS experiments should be satisfactory proxies for the those in the molten state as well. However, this is not actually known. First-principles molecular-dynamics simulations have shown that the structure of a silicate melt (Si—O coordination number) changes as a function of pressure (Karki and Stixrude, 2005). The coordination changes from 4 to 6 gradually throughout the mantle, not as a rapid structural change. Therefore, it is not clear that a quenched glass in the diamond anvil cell will show the same structural signature as a quenched silicate melt that has equilibrated with the metal. Since the iron isotopes are sensitive to the structure of the Fe in the melt, it is important to compare the two systems. And lastly, it is unclear if at high pressure and temperature there is an anharmonicity that is not being accounted for in the data reduction that could affect the fractionation factors determined by NRIXS (Polyakov, 1998).

2.3. Demonstrating equilibrium in experiments

It has been suggested that the best way to prove isotopic equilibrium in high temperature experiments is with the use of the three-isotope technique (Shahar et al., 2008). However, two recent papers have suggested that the technique is not sound. Below, we argue that the technique is solid and in practice is not plagued by the pitfalls described by Cao and Bao (2017), and Bourdon et al. (2018).

Cao and Bao (2017) have argued that the three-isotope method is unlikely to yield equilibrium isotope fractionation factors in general. Their arguments are mainly relevant for the exchange of oxygen isotopes between minerals and liquid or vapor water where fractionations are on the order of 10‰. In what follows we show that the three-isotope method is likely to yield equilibrium fractionation factors for non-traditional stable isotope fractionation at high temperatures with specific reference to Fe isotopes, the arguments by Cao and Bao notwithstanding. We use the kinetic formalism for isotope exchange used previously by Northrop and Clayton (1966) and Criss et al. (1987) and adopted by Cao and Bao.

As an example, we consider Fe isotope exchange between two phases, x and y, as might occur in an phase equilibration experiment. The exchange is described by the reaction,

$$^{54}Fe_x + {}^{56}Fe_y \underset{k}{\overset{\alpha_{Eq}k}{\rightleftharpoons}} {}^{56}Fe_x + {}^{54}Fe_y \tag{12}$$

where k is the rate constant for the exchange process with units of s^{-1} and α_{Eq} is the equilibrium isotope fractionation factor equivalent to the equilibrium constant for the reaction in Eq. (12) where a single Fe per formula unit is involved. The fractionation factor is related to the isotope ratios for the two phases according to

$$\alpha_{Eq} = K_{Eq} = \frac{[^{56}Fe_x][^{54}Fe_y]}{[^{54}Fe_x][^{56}Fe_y]} = \frac{(^{56}Fe/^{54}Fe)_x}{(^{56}Fe/^{54}Fe)_y} = \frac{R_x}{R_y} \tag{13}$$

The tenants of non-equilibrium thermodynamics stipulate that rates of reaction sufficiently close to equilibrium are linear functions of the departures from equilibrium (rates depend on the reaction affinity) (DeGroot and Mazur, 1962). Isotope exchange is such a circumstance and we expect the rates of isotope exchange to be linear functions of the departures of isotope ratios from the equilibrium fractionation factor α_{Eq}. The rate of change of $^{56}Fe/^{54}Fe$ for phase x, R_x, in accordance with Eq. (12), is therefore

$$\frac{dR_x}{dt} = \alpha_{Eq}k\,R_y - k\,R_x \tag{14}$$

such that a steady state at equilibrium is achieved when R_x and R_y attain their equilibrium values, as evident by recognizing that $\alpha_{Eq} = R_{x,Eq}/R_{y,Eq}$, leading to the right-hand side of Eq. (14) being zero. Eq. (14) assumes that the rate is relative to a fixed iron concentration in both phases, and is equivalent to including a fixed $[^{54}Fe_y]$, for example, in the pseudo first order rate constant k. In addition to Eq. (14) the R_x ratio is influenced by the closed-system constraint (mass conservation) imposed by exchange between phases x and y:

$$X_x\frac{dR_x}{dt} + X_y\frac{dR_y}{dt} = 0 \tag{15}$$

where X_x and X_y are the fractions of total Fe in the system hosted in phases x and y, respectively. This closed-system constraint codifies the fact that the phase with the least amount of analyte (Fe in this case) experiences the largest shifts in isotope ratios upon exchange and vice versa. Combining Eqs. (14) and (15) results in

$$\frac{dR_y}{dt} = -k\frac{X_x}{X_y}(\alpha_{Eq}R_y - R_x) \tag{16}$$

and dividing through by (α_{Eq} R_y - R_x) and multiplying through by dt yields

$$\int_{R_y^o}^{R_y(t)} \frac{dR_y}{\alpha_{Eq}R_y - R_x} = \int_{t=0}^{t} -k\frac{X_x}{X_y}dt \tag{17}$$

where R_y^o is the initial ratio and $R_y(t)$ is the final ratio at time t. Upon integration one obtains

$$\frac{1}{\alpha_{Eq}}\ln(\alpha_{Eq}R_y - R_x)\Big|_{initial}^{final} = -k\frac{X_x}{X_y}t \tag{18}$$

or

$$\ln(\alpha_{Eq}R_y - R_x)\Big|_{initial}^{final} = -k\frac{\alpha_{Eq}X_x}{X_y}t \tag{19}$$

Recalling that by definition $\alpha_{Eq} = R_{x,Eq}/R_{y,Eq}$, we have for the left-hand side of Eq. (19) that $\ln(\alpha_{Eq}\ R_y - R_x) = \ln(R_{x,Eq} - R_x)$. Eq. (19) therefore becomes

$$\ln\left\{\frac{R_{x,Eq} - R_x(t)}{R_{x,Eq} - R_x^o}\right\} = -k\,t\left\{\frac{\alpha_{Eq}X_x}{X_y}\right\} \tag{20}$$

Previous workers have found it valuable to convert the ratio on the left-hand side of Eq. (20) to a function of the fractional approach to equilibrium for phase x, f_x, with a range of 0 to 1 from the initial state to equilibrium (e.g., Criss et al., 1987). This is accomplished by recognizing that

$$\frac{R_{x,\mathrm{Eq}} - R_x(t)}{R_{x,\mathrm{Eq}} - R_x^o} = 1 - \frac{R_x(t) - R_x^o}{R_{x,\mathrm{Eq}} - R_x^o} = 1 - f_x \tag{21}$$

Rewriting the isotope ratios in Eq. (21) in terms of fractional differences from a reference ratio, expressed as delta values, such that $R_x(t) = R_{x,\mathrm{ref}}(\delta_x(t) + 1)$, $R_{x,\mathrm{Eq}} = R_{x,\mathrm{ref}}(\delta_{x,\mathrm{Eq}} + 1)$ and $R_x^o = R_{x,\mathrm{ref}}(\delta_x^o + 1)$ one finds that $f_x = (\delta_x(t) - \delta_x^o)/(\delta_{x,\mathrm{Eq}} - \delta_x^o)$. Substitution of Eq. (21) into Eq. (20) leads to the equation relating the fractional approach to equilibrium as a function of time subject to the closed-system constraint:

$$f_x = \frac{\delta_x(t) - \delta_x^o}{\delta_{x,\mathrm{Eq}} - \delta_x^o} = 1 - \exp\left(-k\,t\frac{\alpha_{\mathrm{Eq}}(1 - X_y)}{X_y}\right) \tag{22}$$

Eq. (22) can be written for the two iron isotope ratios $^{56}Fe/^{54}Fe$ and $^{57}Fe/^{54}Fe$, allowing depiction of the evolution of the exchange of iron isotopes in a three-isotope exchange experiment. By ratioing the equations for f_x^{56} and f_x^{57} one obtains the equation for the slope traced by phase x in iron three-isotope space ($\delta^{56}Fe$ as the ordinate vs $\delta^{57}Fe$ as the abscissa) as exchange with phase y proceeds:

$$S_{\mathrm{observed}} = \frac{\delta_x{}^{56}\mathrm{Fe}(t) - \delta_x{}^{56}\mathrm{Fe}^o}{\delta_x{}^{57}\mathrm{Fe}(t) - \delta_x{}^{57}\mathrm{Fe}^o} \tag{23}$$

where S_{observed} is the slope in three-isotope space defined by the data for phase x obtained for different durations of exchange. We note that the mechanism of exchange is not prescribed by these equations, and these mechanisms include heterogeneous reactions driven by chemical potential gradients that result in new mineral growth as well as simple isotope exchange. At issue is how the observed slope defined by the data compares with the "true" slope defined by the line connecting the initial isotopic composition to that defined by equilibrium with phase y. The true slope is defined as

$$S_{\mathrm{true}} = \frac{\delta_x{}^{56}\mathrm{Fe}_{\mathrm{Eq}} - \delta_x{}^{56}\mathrm{Fe}^o}{\delta_x{}^{57}\mathrm{Fe}_{\mathrm{Eq}} - \delta_x{}^{57}\mathrm{Fe}^o} \tag{24}$$

where $\delta_x{}^{56}\mathrm{Fe}_{\mathrm{Eq}}$ is the isotopic delta value prescribed by equilibrium between phases x and y subject to the closed-system constraint. Inspection of Eqs. (22), (23), and (24) shows that the ratio of the slope defined by the data for phase x and the ratio defined by the equilibrium and initial isotope ratios is

$$\frac{S_{\mathrm{observed}}}{S_{\mathrm{true}}} = \frac{f_x^{56}}{f_x^{57}} = \frac{1 - \exp\left(-{}^{56}k\,t\frac{\alpha_{\mathrm{Eq}}^{56}(1 - X_y)}{X_y}\right)}{1 - \exp\left(-{}^{57}k\,t\frac{\alpha_{\mathrm{Eq}}^{57}(1 - X_y)}{X_y}\right)} \tag{25}$$

The observed and true slopes in three-isotope space will be identical when the fractional approaches to equilibrium are the same for both the $^{56}Fe/^{54}Fe$ and $^{57}Fe/^{54}Fe$ ratios for phase x with time. This in turn suggests that the rate constants for exchange for the two isotope ratios, ^{56}k and ^{57}k, are indistinguishable, although Eq. (25) shows that this requirement diminishes with time. The relationship between slopes in three-isotope space is shown in Fig. 1.

The magnitude of the inequality in rate constants can be assessed by considering the isotope selective reaction mechanisms in the experiments. The chemical potential gradients that drive new mineral growth are unlikely to cause significant isotope selectivity in rates. Isotope diffusion in the reactant mineral phases should cause the largest isotope-specific rates of reaction. Even where isotope selectivity at mineral surfaces can occur during reactions, manifestation of the isotopic effects on rates requires diffusion of the isotope fractionation signal into the reactants. Otherwise, the reactant surfaces retreat with no bulk isotope effect. This is a well-known effect exemplified most clearly during sublimation in which diffusion within the condensed phase is required for surface isotope effects to have any influence on the outcome (Young et al., 1998). We expect, therefore, that the largest departures from unity for the ratio $^{56}k/^{57}k$ is where $^{56}k/^{57}k = {}^{56}D/{}^{57}D$, i.e. where the

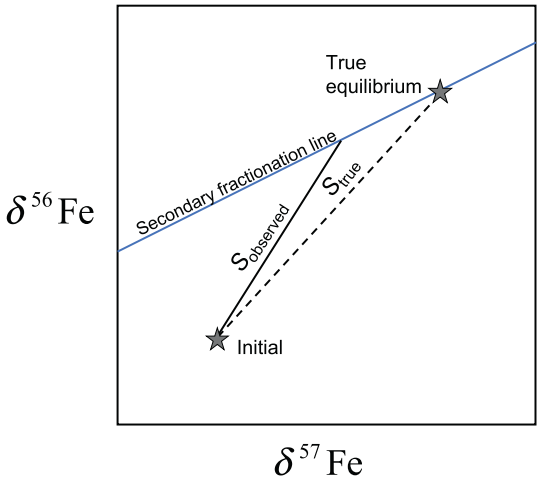

Fig. 1. Schematic Fe three-isotope plot showing the relationships between the observed and ideal, or "true", three-isotope slopes for a single phase experiencing isotope exchange. The true slope is defined by the initial isotopic composition and the true equilibrium value that lies on the secondary fractionation line.

ratio of rate constants is the ratio of the two diffusion coefficients for ^{56}Fe and ^{57}Fe (the diffusivity of ^{54}Fe cancels in the ratio of ratios). In general, the ratio of diffusivities is given by

$$\frac{{}^iD}{{}^jD} = \left(\frac{m_j}{m_i}\right)^\beta \tag{26}$$

m_j and m_i are the masses of the two diffusing species i and j and exponent β is usually ≤ 0.5. For cation diffusion in solids, β is generally $< < 0.5$. In the case of iron, Sio et al. (2018) found that $\beta = 0.16 +/- 0.09$ for Fe isotopes in olivine with compositions with up to 17% Fe relative to Mg, but with values ranging from 0.16 to as low as 0.03 for some crystallographic directions for the more Mg-rich compositions.

In the example that follows we use the exponent of 0.16 to derive a value for $^{56}D/^{57}D$ of 1.00284. This value is taken to be an approximate maximum value for $^{56}k/^{57}k$ in an Fe high-temperature three-isotope exchange experiment. This ratio of rate constants translates into time-dependent values for $S_{\mathrm{observed}}/S_{\mathrm{true}} = f_x^{56}/f_x^{57}$. The variation in this ratio of slopes in three-isotope space with time is shown in Fig. 2 where one sees that the maximum $S_{\mathrm{observed}}/S_{\mathrm{true}}$ of ~1.0045 at the start of the exchange experiment declines as exchange proceeds. After approximately one e-folding time (^{56}k is the reciprocal of the e-folding time for reaction), the departure from the true slope decreases by a factor of 2. After several e-folding times for exchange the departures from the true slope in three-isotope space disappear, meaning that the experiments with closest approaches to equilibrium (where $t\,{}^{56}k > \sim 3$) are least affected by the different isotope-specific rate constants.

The effect of the departures in slope due to isotope-specific rate constants in our example can be examined by comparing the observed $\delta_x{}^{56}Fe$ values to those expected for the ideal case where $S_{\mathrm{observed}}/S_{\mathrm{true}} = 1$. Eqs. (24) and (25) provide the expression for the observed $\delta_x{}^{56}Fe$ values for this comparison:

$$\delta_x{}^{56}\mathrm{Fe}(t)_{\mathrm{observed}} = \delta_x{}^{56}\mathrm{Fe}^o + (\delta_x{}^{57}\mathrm{Fe}(t) - \delta_x{}^{57}\mathrm{Fe}^o)S_{\mathrm{true}}\frac{{}^{56}f_x}{{}^{57}f_x} \tag{27}$$

All of the equations thus far were written for the isotope ratios for phase x, which we take as the spiked phase in our example (e.g., Fig. 1). Analogous expressions apply to phase y, the unspiked reactant in our example. Fig. 3 shows the variations in $\delta_x{}^{56}Fe_{\mathrm{observed}} - \delta_x{}^{56}Fe_{\mathrm{ideal}}$ and $\delta_y{}^{56}Fe_{\mathrm{observed}} - \delta_y{}^{56}Fe_{\mathrm{ideal}}$ as functions of the fractional approach to equilibrium in our example. The largest departures from the ideal case are on the order of 0.01‰ and occur at about 60% exchange.

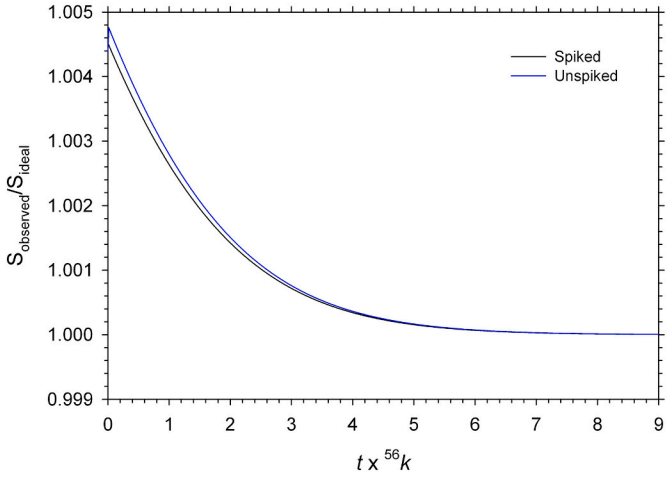

Fig. 2. Calculated ratio of observed three-isotope slope to the true or "ideal" isotope slope as a function of time. The time coordinate is in units of the e-folding time for the exchange rate constant for $^{56}Fe/^{54}Fe$ exchange defined by ^{56}k (s^{-1}). The departure of the observed from the ideal slope diminishes with time. Curves are shown for the unspiked and spiked phases, represented by phases *x* and *y* in the text. This calculation is for Fe divided equally between the two phases ($X_x = X_y = 0.5$).

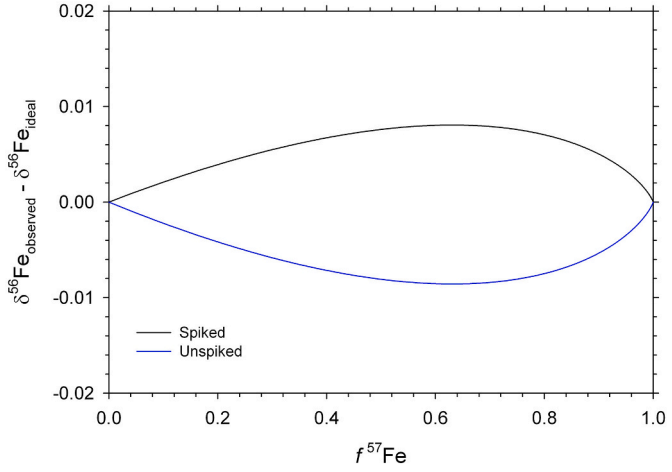

Fig. 3. The difference in the $\delta^{56}Fe$ for two phases exchanging isotopes as a function of the degree of equilibration $f\ ^{57}Fe$ for $^{57}Fe/^{54}Fe$. The calculation is for the example described in the text in which the total Fe in the system is divided equally between the two phases and the exchange kinetics is controlled by diffusion. Note the magnitude of the discrepancy caused by the different diffusivities of ^{56}Fe and ^{57}Fe and the shape of the distributions.

How do these differences in rate constants affect the final results? In order to illustrate the answer to this question we chose six samples representing a reactant (phase *x*) spiked with excess ^{54}Fe at six different durations of exchange and the six corresponding samples of the unspiked reactant (phase *y*) from our numerical example described above. The amount of ^{54}Fe spike and the six different degrees of exchange are similar to those in the 600 °C experiments for Fe isotope exchange between magnetite and fayalite from Shahar et al. (2008). We assigned 1 σ uncertainties of +/−0.01‰ and +/−0.002‰ to the $\delta^{56}Fe$ and $\delta^{57}Fe$ values, respectively, in keeping with typical iron isotope ratio measurement uncertainties. For this example, similar to the actual experiments, $Xx = Xy = 0.5$. The results are shown in Fig. 4. As usual in the three-isotope method, the example fictive data were regressed and the values for $\alpha_{Eq}{}^{56}$ and $\alpha_{Eq}{}^{57}$ obtained from the intersections of the best-fit lines with the secondary fractionation line. The uncertainties in the derived equilibrium fractionation factors correspond to the intersections of the error envelopes for the best fits with the secondary fractionation line. The value for $\delta^{56}Fe_{spiked} - \delta^{56}Fe_{unspiked}$, corresponding to $\sim 10^3\ \ln(\alpha_{Eq}{}^{56})$, is −0.284 +/− 0.053 (1 s) ‰. This compares with the true or ideal value not affected by the unequal rate constants of −0.272 +/− 0.054‰. Clearly, in this example the effect of unequal rates of exchange caused by different diffusivities in the exchanging phases makes only a negligible difference in the result (Fig. 4).

Cao and Bao (2017), noted that because the equilibrium fractionation factors also influence the rates of reaction (they appear in Eq. (14)), unequal fractional approaches to equilibrium for the two isotope ratios comprising a three-isotope system are inevitable. However, in practice, the fractionation factors at higher temperatures are sufficiently close to unity that this effect is entirely negligible. We included the different equilibrium fractionation factors in our implementation of Eq. (25) in the example described above, confirming this expectation.

The discrepancy between the observed and true values in the above example are not terribly disquieting given uncertainties in such experiments, and we suggest that since the $^{56}k/^{57}k$ employed here is something of a maximum, this is about as poor as such experiments would get. This simple set of calculations demonstrates that while the possibility for unequal rates of exchange can affect results in principle, in practice the effects are rather small for well-designed experiments (i.e., those that do not introduce multiple exchange pathways that are kinetically limited).

We point out that Lazar et al. (2012) investigated many of the confounding issues raised by Cao and Bao, including the effects of loss of analyte to a third phase (e.g., capsule walls in an experiment). In Fig. 9 of that paper the linearity of the exchange path in Ni three-isotope space was examined. The exchange was found to be linear within uncertainties after a brief interval of "adjustment." The Ni isotope exchange experiments comprise empirical evidence that the reaction rates do not differ enough to be detectable, at least for this system. This is evidence that measurable deviations from a linear exchange path are not inevitable.

The discussion to this point has concentrated on rates of isotope exchange. However, in our experience, most successful three-isotope experiments involving non-traditional stable isotopes exchanged between solid phases at high temperatures involve new mineral growth. Indeed, the experiments are designed to cause new mineral growth to surmount the hurdle of slow diffusion of the analyte species. In these cases, it is likely that the newly grown minerals are at, or very near to, isotopic equilibrium. The slopes in three-isotope defined by the data are in these cases mixing lines between the starting material and the equilibrated material. The greater the extent of new mineral growth, the closer the sample appears to isotopic equilibrium. As shown in Fig. 3, mixing between starting material and fully equilibrated sample will define the ideal, or true, slope in three isotope space (e.g., mixing between the two ends of the abscissa in Fig. 3), essentially bypassing any kinetically-induced deviations from S_{true} and eliminating the potential for spurious slopes that could cause incorrect equilibrium fractionation factors. A recent study by Trail et al. (2019) shows evidence for this regrowth in three-isotope experiments involving exchange of Si isotopes between quartz and zircon, and previous studies (Shahar et al., 2008; Macris et al., 2013) had shown similar textural evidence for regrowth accommodating equilibration.

Bourdon et al. (2018) examined the consequences of altering X_y and, by difference, X_x, the fractions of the analyte partitioned between the two phases in a three-isotope exchange experiment, as a result of mineral growth or changes in mineral chemistry. This will be an issue most likely where the element of interest is a minor or trace component in one of the phases (Si in Fe metal is an obvious example) and the initial reactant phase does not contain the equilibrium concentration of the element of interest and thus its concentration in that phase changes during the experiments. While efforts are made to avoid this circumstance by choosing suitable reactants, numerical implementation of the

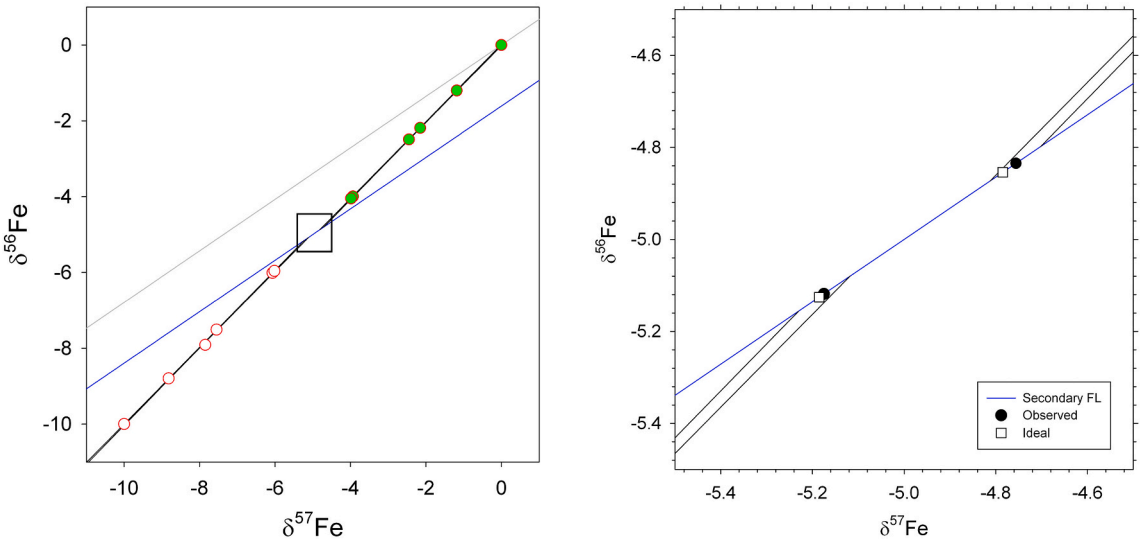

Fig. 4. Results of a numerical simulation of a three-isotope exchange experiment in the Fe isotope system, as described in the text. Exchange is between a reactant spiked with excess ^{54}Fe and an unspiked reactant. The ratio $^{56}k/^{57}k$ is set equal to the ratio of diffusivities for ^{56}Fe and ^{57}Fe, and is 1.00284. Degrees of equilibration, the distribution of Fe between the two reactants, and the fictive measurement uncertainties are taken to be similar to those in the experiments reported by Shahar et al. (2008). The error bars for the individual fictive data points are smaller than the symbols. The left panel shows the data together with the secondary fractionation line (blue) and the terrestrial fractionation line (grey). The spiked fictive reactants, below the secondary fractionation line, are shown as white circles while the unspiked reactants above the secondary fractionation line are shown as green circles. The panel on the right is a closeup (range indicated by the box in the left panel) showing the intersections of the 1σ error envelopes for the ficitive spiked and unspiked data. The true, or ideal, δ^{57}Fe and δ^{56}Fe values for this example are shown by the white squares while the intersections obtained by the best fits to the data are shown by the black circles. Note that the intersections defined by the data are within error of the true (ideal) values.

equations derived above shows that marked departures from linearity in three-isotope space are not expected even where large shifts in apportioning of the analyte element occur. Fig. 5 shows one such calculation in which the fraction of total Fe contained within the unspiked phase (starting out above the secondary fractionation line) varies from 0.2 to 0.5. Following the suggestion by Bourdon et al., we varied X_y according to $X_y(t) = X_y^{\text{final}} + (X_y^{\text{initial}} - X_y^{\text{final}})\ \exp.(-t^{56}k/\tau_{\text{chemical}})$ where τ_{chemical} is the time constant for chemical exchange relative to the time constant for isotopic exchange (taken as $1/^{56}k$). For this example, the time constant for chemical exchange was taken to be 3 times that for isotopic exchange, the δ^{57}Fe fractionation between the two phases is 0.4‰, and the bulk system has δ^{57}Fe and δ^{56}Fe values of −5 and − 6‰, respectively. One sees that departures from linearity are negligible until > 90% exchange is attained, and even then, the separation between the two phases records the actual fractionation. Shorter time constants for chemical exchange lead to more direct pathways to the equilibrium isotope ratios while longer time constants lead to sharper turns onto the secondary fractionation line than shown in Fig. 5. In the worst case, the chemical time constant is greater than the isotope exchange time constant, and one phase is sampled close to the secondary fractionation line while the other far from the line. This would cause an error on the order of 0.1‰ at most. What is more, since, as described above, it is likely that experimental products will be mixtures of unreacted starting material and nearly equilibrated products, linear mixing trends that extrapolate to equilibrium in three-isotope space are expected. In their analysis, Bourdon et al. considered the possibility that chemical disequilibrium would be accompanied by isotope-specific reaction rate constants scaled by the inverse of the square root of masses. However, as mentioned above, it is not clear that net-transfer reactions driven by gradients in bulk chemical potentials are accompanied by such large isotopic effects.

There are important validations of the three-isotope method that should be considered when evaluating the veracity of the results. For example, Ziegler et al. (2010) show in their Fig. 1 the remarkable agreement for ^{30}Si/^{28}Si fractionation between metal and silicate between theory, three-isotope measurements from Shahar et al. (2009), and measurements in meteorites. This is very unlikely to be a coincidence. Similarly, Fig. 5 from Macris et al. (2013) shows that the three-isotope method for Mg isotope exchange amongst carbonate, spinel, and forsterite defined fractionation factors indistinguishable from theory. Forsterite-magnesite is an exception, but the difference is small in view of the uncertainties and the problem is most likely to do with the calculations for carbonates rather than with the measurements. Also, Roskosz et al. (2015) confirmed the three-isotope experimental data for equilibrium Fe isotope fractionation between magnetite and fayalite of Shahar et al. (2008) using reduced partition functions from NRIXS (see their Fig. 5). What is more, Hill et al. (2009) found agreement between theory and three-isotope measurements of equilibrium fractionation factors between various aqueous ferric chloride complexes and $FeCl_4^-$ in the Fe isotope system at lower temperatures.

Based on the calculations and the examples cited above, there is clear evidence that the three-isotope method as applied to non-traditional stable isotopes at high temperatures can be used to measure equilibrium fractionation factors successfully. In making the determination of the overall veracity of the method, one must be careful about ascribing significance to disagreements between experiments and theory and between experiments and data from natural systems. For example, we must be mindful of the fact that the purpose of doing the experiments is to confirm or contravene predictions based on theory; where theory and measurements disagree, it is not clear a priori which one is in error. Ideally, theory would be sufficient. However, experience shows that this is all too often not the case. The Fe isotope results for magnetite and fayalite are an illustrative example. The disagreement between the three-isotope-derived equilibrium fractionation factor by Shahar et al. (2008) and the force-constant predictions from Polyakov et al. (2007) and Polyakov and Mineev (2000) could have been taken as potential evidence for failure of the three-isotope method. But the more recent force-constant measurement by NRIXS (e.g. Liu et al., 2017) is consistent with the three-isotope determination. The details of how to reduce the force-constant data come into play here. Similarly, measurements in natural samples may or may not represent equilibrium. Indeed, the point of experiments is to establish equilibrium

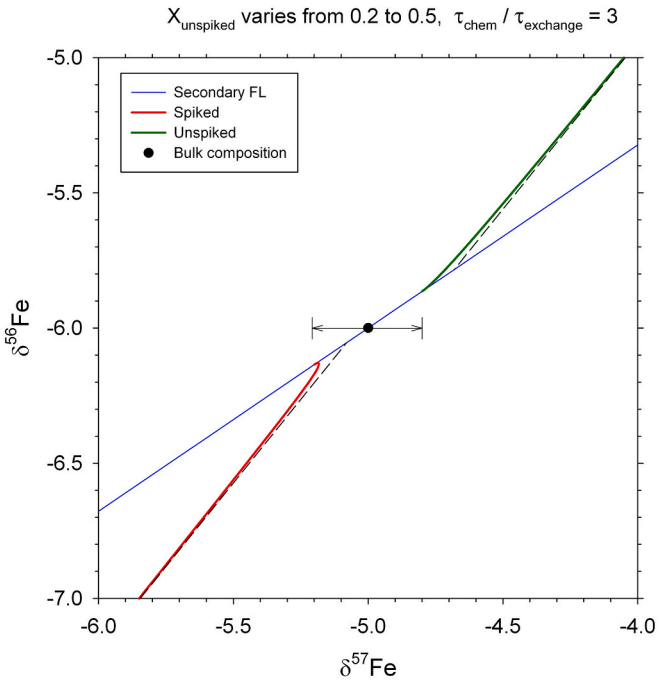

Fig. 5. Calculation of three-isotope exchange of Fe isotopes between a ^{54}Fe spiked phase and an unspiked phase. The fraction of total Fe contained within the unspiked phase, X_y, varies during exchange from 0.2 to 0.5 using $X_y(t) = X_y^{\text{final}} + (X_y^{\text{initial}} - X_y^{\text{final}})\exp.(-t\,^{56}k/\tau_{\text{chemical}})$ where τ_{chemical} is the time constant for chemical exchange relative to the time constant for isotopic exchange (the latter is $1/^{56}k$). In this calculation the time constant for chemical exchange was taken to be 3 times that for isotopic exchange, the δ^{57}Fe equilibrium fractionation between the two phases is 0.4‰, and the bulk system has δ^{57}Fe and δ^{56}Fe values of −5 and − 6‰, respectively. The black dot is the bulk composition for the system. The double arrow shows the equilibrium ^{57}Fe/^{54}Fe (δ^{57}Fe) fractionation between the two phases. Dashed lines are the slopes corresponding to a constant X_y of 0.2 with no change during exchange for reference.

fractionation values so that the observations in the field can be interpreted.

Finally, the recent study by Trail et al. (2019) showed experimentally that the three-isotope technique provided the best indicator of the silicon equilibrium fractionation between quartz and zircon, while experiments that did not use the technique provided a false equilibrium fractionation factor. We, therefore, suggest that the three-isotope method does provide accurate estimates of equilibrium fractionation factors for Fe isotope fractionation between phases and those of other non-traditional stable isotopes at high temperatures if experiments are designed properly.

3. Results of metal-silicate experiments

Elardo et al. (2019) did a thorough investigation into why experiments aimed at understanding iron isotope fractionation during core formation at high pressure and temperature show a large scatter. Fig. 6 shows a compilation of all published experiments. The results show a large range that suggests at first glance profound disagreements. However, the disagreements are not as vexing when one considers the many ways in which experiments are not comparable (Elardo et al., 2019). Perhaps of paramount importance are differences in composition. Therefore, there should be caution taken when comparing published iron isotope exchange experiments.

As an illustration of the importance of composition, Fig. 7 shows results of published experiments for Fe isotope exchange between metal and silicate replotted as a function of the total substitutional impurities in the metal (nickel, sulfur, and silicon), and with experiments with no indications of achieving equilibrium removed. In Fig. 6, there are 38 experiments plotted, but in Fig. 7 we only plot 19 experiments. The other half were omitted from the trend for the following reasons. The one experiment from Roskosz et al. 2006, was removed as it proved difficult to disentangle kinetic and equilibrium effects from the fractionation factor. Experiment PC978 from Shahar et al., 2015, was omitted as the run products showed olivine as well as silicate melt. All the Hin et al., 2012 data were omitted as their results are difficult to interpret, as discussed in greater detail in Elardo et al., 2019. In particular, their results had large amounts of tin within the metallic phase, not only changing the structure, but also the phase relations. Based on phase relations it is likely that the run products had more than one metallic phase during the experiment. Further, as discussed in great detail earlier, proving equilibrium is not simple and these experiments did not show that their experiments had equilibrated. It is just not possible to compare experiments when the reason for using a fusible element in the metal is to change the melting temperature of the melt, as by definition, that changes the structure of the metallic melt. We strongly urge the community not to use tin in future experiments for these reasons. It is not difficult to use more realistic compositions. Lastly, there is only one experiment plotted from the Poitrasson et al., 2009 study. The one experiment that is plotted is the one that had a run duration of 30 min, the longest in the study. Based on previous experiments, it has been shown that experiments cannot equilibrate as quickly as the duration of most of the experiments in that study. Therefore, only the 19 experiments that clearly show a closed system, only two phases, and high probability of equilibrium have been plotted.

When the data are then plotted this way, a more coherent story emerges. It is now clear that there is in fact an iron isotope fractionation between metal and silicate at high temperature and 1 GPa (e.g. Elardo et al., 2019), however, the details of the fractionation depend on composition. This is not surprising since composition affects bond properties, and the properties of the bonds (e.g., bond stiffness) control vibrational properties that in turn control the relative proclivity of a phase for heavy or light isotopes. The composition of the metal, in particular, appears to have a large effect on the Fe isotope fractionation between silicates and metal, depending on which element(s) is bonded to the iron (Fig. 7). In the experiments conducted thus far, silicon, nickel, and sulfur have been shown to effect this fractionation.

All of the experiments discussed above were conducted in the piston cylinder apparatus where both metal and silicate phases equilibrate in the molten state. Results for silicate-metal Fe isotope fractionation using NRIXS are fundamentally different and at first glance show a much different picture with regards to isotope fractionation during core formation. Fig. 8 shows the apparent discrepancy between the NRIXS experiments and the piston cylinder experiments. The NRIXS data all cluster around 0 permil fractionation between metal and silicate whereas the piston cylinder experiments show a trend as a function of the light element alloyed with the iron metal. It has been argued that the discrepancy between metal and silicate Fe isotope fractionation obtained using NRIXS and that obtained using experiments in the piston cylinder using the three-isotope technique is due to perceived limitations of the three-isotope method (Bourdon et al., 2018). We point out, however, that there are no data to support that claim. We find instead that the problem most likely is insufficient attention to the effects of impurities in the metals in the various experiments.

This is seen clearly in Fig. 9 where only the data from Fig. 8 that do not have substitutional elements within the iron structure are shown. When confined to these data only, there is considerable agreement between the piston cylinder experiments and the NRIXS experiments; the two methods agree when the iron in the experiment is pure or alloyed with an interstitial element such as carbon rather than a substitutional element. Interestingly, the average value for the iron isotope fractionation between metal and silicate in these experiments is negative, suggesting that the silicate is more enriched in the heavy isotopes relative to the metal at these conditions. However, it seems that the

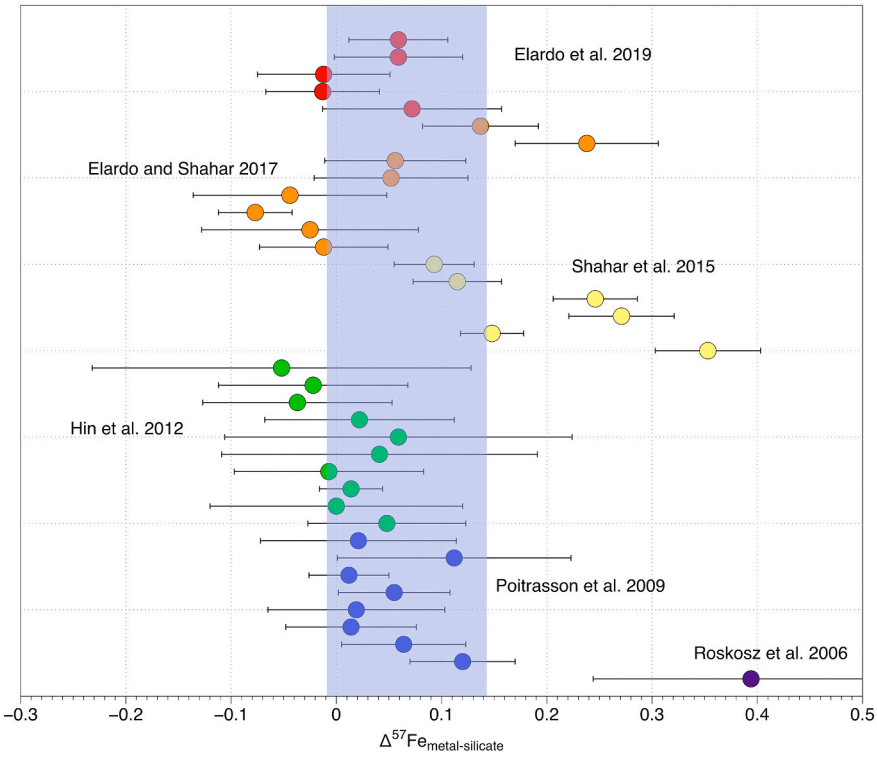

Fig. 6. A compilation of all piston-cylinder and multi-anvil experiments conducted in the metal/silicate system corrected to the same temperature, 1850 °C. Colors correspond to different literature data (from the top – red - Elardo et al., 2019; orange - Elardo and Shahar, 2017; yellow - Shahar et al., 2015; green - Hin et al., 2012; blue - Poitrasson et al., 2009; purple - Roskosz et al. 2006). The shaded bar represents the average for all of these experiments and the errors are all 2SE.

fractionation changes sign as substitutional elements are alloyed with iron. For an unknown reason, the NRIXS experiments with substitutional alloys ($Fe_{86.8}Ni_{8.6}Si_{4.6}$, $Fe_{85}Si_{15}$, Fe_3S, $Fe_{92}Ni_8$, Liu et al., 2017) are the only ones that do not agree with this piston cylinder trend. It is not clear why these samples do not show a fractionation associated with the alloying of iron, similar to those in the piston cylinder experiments. Possible reasons for this discrepancy include anharmonicity at high pressure and temperature for these phases, causing the force constant determinations to be inaccurate, an inhomogeneous sample quench, or another yet to be determined cause.

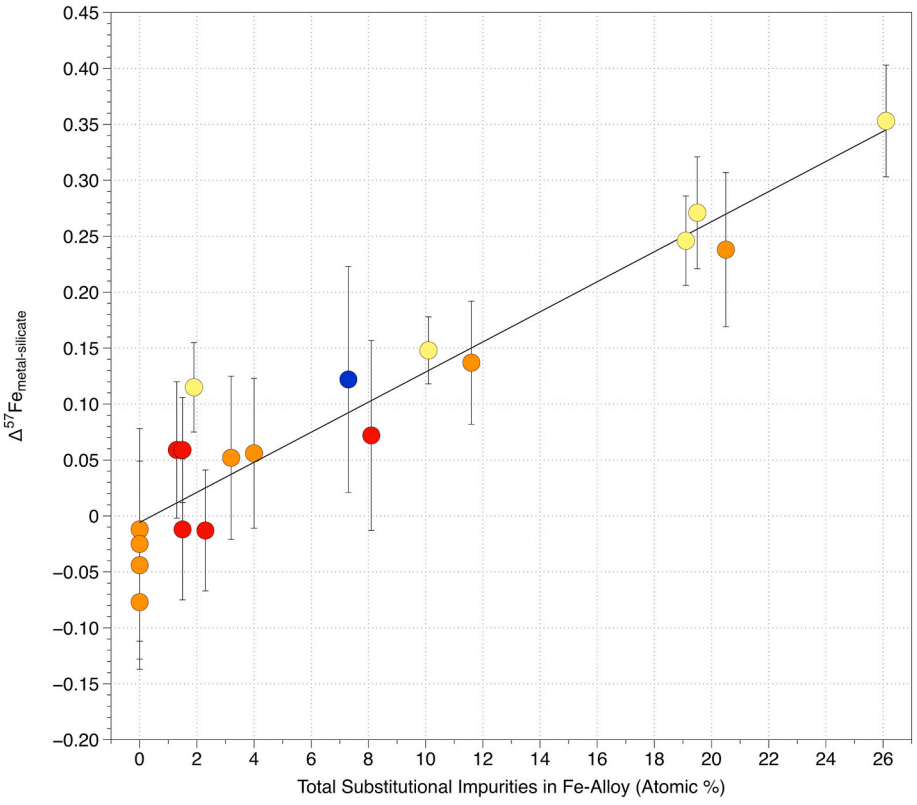

Fig. 7. A compilation of all piston-cylinder and multi-anvil experiments conducted in the metal/silicate system corrected to the same temperature and including only those experiments shown to have come to equilibrium (as described in the text) plotted against the total substitutional impurities present in the Fe-alloy in each experiment. The best fit line through all the experiments goes through the origin and has an R^2 value of 0.895. Colors represent different studies as in Fig. 6.

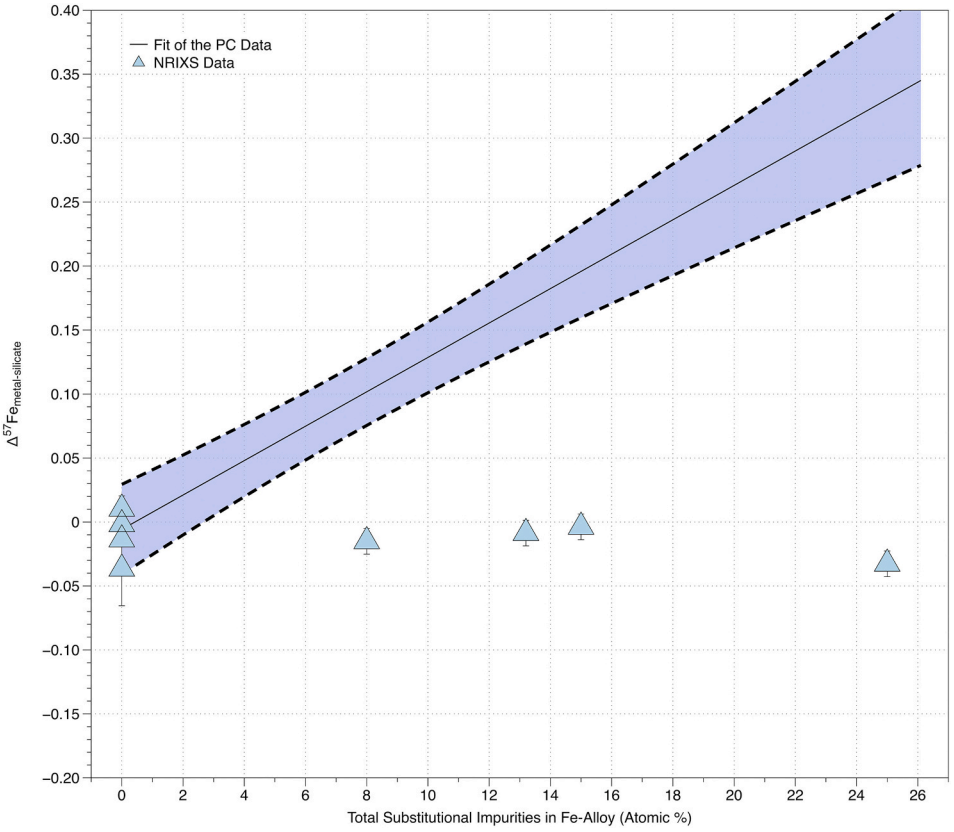

Fig. 8. The range of piston cylinder experiments shown in Fig. 7 as well as data from NRIXS experiments corrected to the same pressure and temperature as the piston cylinder experiments, 1 GPa and 1850 °C, showing an apparent discrepancy. Data for NRIXS experiments are from Shahar et al., 2016 and Liu et al., 2017. NRIXS errors in most cases are smaller than the symbol. Note that it is rare to nature to find iron that is pure and not alloyed to nickel. Note that it is rare to nature to find iron that is pure and not alloyed to nickel.

4. Implications for Earth and other planetary bodies

Based on all the experimental data summarized above, it is clear that there is an equilibrium iron isotope fractionation between metal and silicate when the composition of the metal is alloyed with substitutional elements, such as nickel. Further, this fractionation has been shown to change with temperature, pressure, and composition of the metal and silicate (as well as the Fe^{3+} content of the silicate, Dauphas

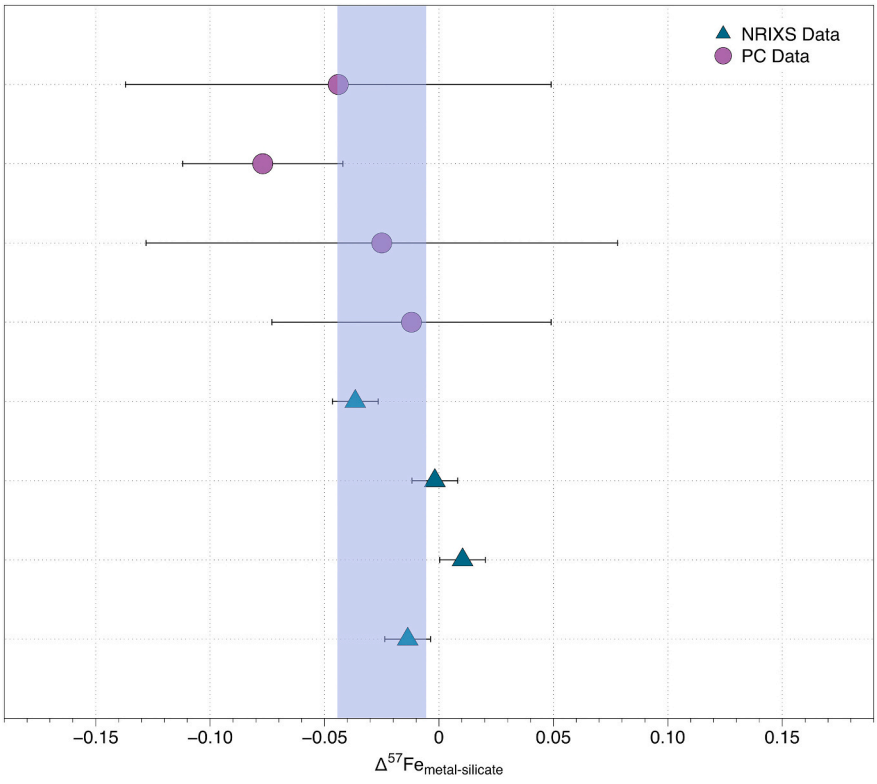

Fig. 9. All the data plotted in Fig. 8 with no substitutional elements alloyed to the iron metal. These data are from both NRIXS (triangles) and piston cylinder (circles) experiments. The shaded bar is the mean of the data with the 2SE of the mean. When plotted this way it is clear that there is no discrepancy amongst the two techniques and that there is even a hint of a negative average fractionation between metal and silicate when the iron is pure.

et al., 2014). Note that it is rare in nature to find iron that is pure and not alloyed to nickel. Therefore, it is important to assess whether the conditions during core formation were such that the fractionation would be exhibited by natural samples today. The fractionation would be negligible and not resolvable if the temperatures of equilibration were too high, for example. Taken at face value, the piston cylinder experiments and NRIXS data suggest that:

1. In a *pure* iron-silicate system the $\Delta^{57}Fe_{metal\text{-}silicate}$ fractionation is slightly negative at low-pressures, implying that the silicate is isotopically heavier than the metal.
2. Where the iron is alloyed with substitutional elements at low pressure, such as nickel or sulfur, the sign of $\Delta^{57}Fe_{metal\text{-}silicate}$ changes to positive and the metallic alloy has higher $^{57}Fe/^{54}Fe$ than silicate at equilibrium.
3. At high pressures relevant to Earth's core formation, $\Delta^{57}Fe_{metal\text{-}silicate}$ is always negative, and silicate is isotopically heavier than coexisting metal, regardless of the composition of the metal phase.
4. There is an increase in the equilibrium metal-silicate Fe isotope fractionation with pressure, but this effect is negligible below ~5–10 GPa.
5. As temperature increases, the fractionation decreases in all systems and trends towards zero.

Difficulties arise in applying these results because seldom are core and mantle observable in the same body in the solar system. The meaning of the observed Fe isotope ratios for the mantle rocks, or metallic cores, must usually be ascertained by assuming values for the whole body. For example, based on these observations, it can be deduced that planetesimals and small-sized planets that have never reached internal pressures of greater than a few GPa should have metal cores that are higher in $^{57}Fe/^{54}Fe$ than their silicate mantles (Elardo and Shahar, 2017; Elardo et al., 2019). This is not only due to the size of the planet but also to the temperature, as these planetesimals would not have reached very high internal temperatures. Furthermore, as iron seems to always be alloyed with some nickel, the sign of $\Delta^{57}Fe_{metal\text{-}silicate}$ should always be positive for these smaller bodies.

At first this might seem to explain why magmatic iron meteorites, representing the vestiges of cores of smaller planetesimals, are generally higher in $\delta^{57}Fe$ than silicates and oxides in the solar system by an average of about 0.13‰ (Zhu et al., 2002; Kehm et al., 2003; Williams et al., 2005; Dauphas et al., 2009; Craddock and Dauphas, 2011; Jordan et al., 2019). However, if it is assumed that the parent bodies of these cores had bulk $\delta^{57}Fe$ values that were chondritic, then one expects the $\delta^{57}Fe$ of the cores to be very nearly chondritic because the vast majority of the iron is expected to be present in the core rather than in the silicate mantle. The positive $\Delta^{57}Fe_{metal\text{-}silicate}$ fractionation should be manifested as low $\delta^{57}Fe$ in the mantles rather than high $\delta^{57}Fe$ in the cores. Two solutions to this conundrum have been proposed recently. One is fractionation of Fe isotopes between solid and liquid Fe-rich metal, and the other is preferential evaporation of light Fe isotopes from the magmatic iron meteorite parent bodies. Jordan et al. (2019) were the first to quantitatively evaluate these options. By assuming a temperature-independent and composition-independent Fe isotope fractionation factor between solid and liquid metal, the authors found it difficult to simultaneously explain the Fe isotope and trace element trends of the IIIAB irons by fractional crystallization. They concluded that while $\delta^{57}Fe$ in solid Fe-rich metal > $\delta^{57}Fe$ in liquid Fe-rich metal could explain the iron meteorite Fe isotope data in principle, this interpretation was not consistent with trace element indicators for fractional crystallization. They noted that the fact that there is no correlation between $\delta^{57}Fe$ in these rocks with variations in compatible/incompatible trace element ratios over three orders of magnitude meant that fractional crystallization did not alter the $\delta^{57}Fe$ value of the metal core. The authors therefore argued that the heavy Fe isotopes of iron meteorites might be partially due to evaporation during accretion of their parent bodies, although there is no clear evidence for evaporation of other siderophile elements (Luck et al., 2005). A more recent study by Ni et al. (2020) experimentally determined the Fe isotope fractionation between solid and liquid metal in a Fe-Ni-S system directly applicable to the iron meteorites, and found that at ~1500 to 1700 K, solid metal is heavier in $\delta^{57}Fe$ than liquid by 0.1 to 0.2‰ regardless of composition. Moreover, with a modified trapped melt model, the authors were able to simultaneously reproduce the Fe isotope trend and trace element data for IIIAB irons. Therefore, Ni et al. (2020) were able to explain the heavy Fe isotopes of iron meteorites solely by core crystallization. This explanation requires that there is a missing meteorite record of a S-rich reservoir in iron meteorite parent bodies that is enriched in light Fe isotopes.

Planets the size of Earth present the opposite problem in that we sample the silicate and oxide rocks but not the core. Because core formation for Earth and similarly massive planets reached much higher pressures and temperatures, the Fe isotopic effects of core formation will have been smaller and difficult to disentangle from subsequent iron isotope fractionation occurring in the rocks. At the high temperatures envisaged for core formation on Earth (> 3500 K) it is difficult to imagine that an equilibrium iron isotope fractionation would be seen due to core formation unless the core is alloyed with hydrogen, for example (Shahar et al., 2016). If that were the case then the silicate portion of the Earth would be homogeneously enriched in $\delta^{57}Fe$. Mid-ocean ridge basalts, often taken as samplings of mantle in isotope work, are high in $\delta^{57}Fe$ relative to chondrites by ~0.15‰. However, in general, for upper mantle minerals, the relative fractionations are known to be $\delta^{57}Fe$ olivine < $\delta^{57}Fe$ pyroxene < $\delta^{57}Fe$ spinel (Macris et al., 2013), suggesting that partial melting of the mantle that melts the pyroxene component preferentially, will lead to isotopically heavy basalt relative to mantle. This effect must be accounted for when reconstructing the Bulk Silicate Earth $\delta^{57}Fe$. While there is still debate as to what the iron isotopic composition of the BSE is (Craddock et al., 2013; Poitrasson et al., 2013; Sossi et al., 2016), it is likely that Earth's interior is not homogeneous and that post-formation processes have affected that Fe isotopic composition of different portions of the mantle. In all cases, in order to assess the bulk Fe isotopic composition of a rocky planet, one must remove the effects of igneous differentiation.

Core formation has been suggested as a possible reason for the relatively high iron isotope ratios seen in mid-ocean ridge basalts and ocean island basalts (Polyakov, 2009; Teng et al., 2013; Craddock et al., 2013), and disproportionation has been suggested as a cause of iron isotope heterogeneity in the mantle (Williams et al., 2012). However, based on the experimental data obtained thus far both by NRIXS and piston cylinder experiments it is clear that there is no process that occurs at deep mantle temperatures that can account for the $\delta^{57}Fe$ values seen in basalts relative to chondrites. The only caveat is that the iron isotope fractionation associated with partial melting has not been experimentally determined yet, though first estimates from natural samples and NRIXS experiments show that it cannot account for the full fractionation (Dauphas et al., 2014). On smaller planets and differentiated planetesimals, such as Mars and Vesta one would expect that the fractionation seen from core formation would result in a light mantle and heavy core (Elardo and Shahar, 2017). Samples from the silicate portions of these bodies do not show this light signature, assuming they are chondritic in bulk, and it has been proposed that the partial melting effect that raises the $\delta^{57}Fe$ of basaltic crusts could make it appear as though they are still chondritic. It is important to remember that with stable isotopes, there are many chemical and physical processes that can cause the isotopic composition to change and that the ratios analyzed are a sum of all those processes combined.

5. Concluding remarks

Iron has been the archetype system for non-traditional stable isotopes as tracers during planet formation. Many experiments have been

conducted and many samples have been analyzed. In the case of experiments, great care must be taken to ensure that kinetic processes do not prevent equilibrium, and that some method of either verifying equilibrium or extrapolating to equilibrium is used. The three-isotope technique is the most rigorous way to do this. The numerous studies to date show that that stable isotopes of Fe can fractionate in a myriad of high-temperature settings and under many conditions. Disentangling the processes that cause variations in Fe isotope ratios in high-temperature rocks requires a thorough understanding of the isotopic fractionation factors associated with each process. For the iron isotope system it has been made clear in the literature that the equilibrium fractionation factor is a function of pressure, temperature, crystal chemistry, including the valence state of the iron, and composition, at the very least.

During core formation in planetesimals the molten metallic core separates from the molten silicate portion and iron is partitioned into both phases according to the prevailing oxygen fugacity. Resolvable Fe isotope signatures of this process are expected, and are evident in meteoritical samples. In general, δ^{57}Fe of the metal should be greater than that of the rocky mantles for these smaller bodies, but the details depend on the compositions of the metal phases. For Earth, and other rocky planets of comparable or greater mass, the pressures and temperatures attending core formation were high enough that the fractionation will be small compared with our current analytical precision. Nonetheless, the effects are expected to be critically dependent on the composition of the metallic portion of the core, with the silicate generally having higher δ^{57}Fe than the metal.

Declaration of competing interest

The authors declare that they have no known competing financial interests or personal relationships that could have appeared to influence the work reported in this paper.

Acknowledgments

AS acknowledges support from the Carnegie Institution for Science. EDY acknowledges support from the NASA Emerging Worlds grant number 80NSSC19K0511. AS thanks S. Elardo, P. Ni and N. Nie for the thoughtful discussions.

References

Badro, J., Brodholt, J.P., Piet, H., Siebert, J., Ryerson, F.J., 2015. Core formation and core composition from coupled geochemical and geophysical constraints. Proc. Natl. Acad. Sci. 112 (40), 12310–12314.
Beard, B.L., Johnson, C.M., 1999. High precision iron isotope measurements of terrestrial and lunar materials. Geochim. Cosmochim. Acta 63 (11 − 12), 1653–1660.
Beard, B.L., Johnson, C.M., 2004. Fe isotope variations in the modern and ancient earth and other planetary bodies. Rev. Mineral. Geochem. 55 (1), 319–357.
Beard, B.L., Johnson, C.M., Cox, L., Sun, H., Nealson, K.H., Aguilar, C., 1999. Iron isotope biosignatures. Science 285, 1889–1892.
Beard, B.L., Johnson, C.M., Von Damm, K.L., Poulson, R.L., 2003. Iron isotope constraints on Fe cycling and mass balance in oxygenated Earth oceans. Geology 31 (7), 629–632.
Birch, F., 1964. Density and composition of mantle and core. J. Geophys. Res. 69 (20), 4377–4388.
Bourdon, B., Roskosz, M., Hin, R.C., 2018. Isotope tracers of core formation. Earth Sci. Rev. 181, 61–81.
Boyd, F.R., England, J.L., 1960. Apparatus for phase-equilibrium measurements at pressures up to 50 kilobars and temperatures up to 1750° C. J. Geophys. Res. 65 (2), 741–748.
Bullen, T.D., White, A.F., Childs, C.W., Vivit, D.V., Schulz, M.S., 2001. Demonstration of significant abiotic iron isotope fractionation in nature. Geology 29 (8), 699–702.
Cao, X., Bao, H., 2017. Redefining the utility of the three-isotope method. Geochim. Cosmochim. Acta 212, 16–32.
Corgne, A., Siebert, J., Badro, J., 2009. Oxygen as a light element: a solution to single-stage core formation. Earth Planet. Sci. Lett. 288 (1–2), 108–114.
Craddock, P.R., Dauphas, N., 2011. Iron isotopic compositions of geological reference materials and chondrites. Geostand. Geoanal. Res. 35 (1), 101–123.
Craddock, P.R., Warren, J.M., Dauphas, N., 2013. Abyssal peridotites reveal the near-chondritic Fe isotopic composition of the Earth. Earth Planet. Sci. Lett. 365, 63–76.
Criss, R. E., Gregory, R. T., and Taylor Jr, H. P. (1987). Kinetic theory of oxygen isotopic exchange between minerals and water. Geochim. Cosmochim. Acta, 51(5), 1099–1108.
Dauphas, N., Craddock, P.R., Asimow, P.D., Bennett, V.C., Nutman, A.P., Ohnenstetter, D., 2009. Iron isotopes may reveal the redox conditions of mantle melting from Archean to present. Earth Planet. Sci. Lett. 288, 255–267.
Dauphas, N., Roskosz, M., Alp, E.E., Golden, D.C., Sio, C.K., Tissot, F.L.H., Hu, M., Zhao, J., Gao, L., Morris, R.V., 2012. A general moment NRIXS approach to the determination of equilibrium Fe isotopic fractionation factors: application to goethite and jarosite. Geochim. Cosmochim. Acta 94, 254–275.
Dauphas, N., Roskosz, M., Alp, E.E., Neuville, D.R., Hu, M.Y., Sio, C.K., Tissot, F.L.H., Zhao, J., Tissandier, L., Nedard, E., Cordier, C., 2014. Magma redox and structural controls on iron isotope variations in Earth's mantle and crust. Earth Planet. Sci. Lett. 398, 127–140.
Dauphas, N., Hu, M.Y., Baker, E.M., Hu, J., Tissot, F.L., Alp, E.E., Roskosz, M., Zhao, J., Bi, W., Liu, J., Lin, J.F., 2018. SciPhon: a data analysis software for nuclear resonant inelastic X-ray scattering with applications to Fe, Kr, Sn, Eu and Dy. J. Synchrotron Radiat. 25 (5).
DeGroot, S.R., Mazur, P., 1962. Non-Equilibrium Thermodynamics.
Elardo, S.M., Shahar, A., 2017. Non-chondritic iron isotope ratios in planetary mantles as a result of core formation. Nat. Geosci. 10 (4), 317.
Elardo, S.M., Shahar, A., Mock, T.D., Sio, C.K., 2019. The effect of core composition on iron isotope fractionation between planetary cores and mantles. Earth Planet. Sci. Lett. 513, 124–134.
Hill, P.S., Schauble, E.A., Shahar, A., Tonui, E., Young, E.D., 2009. Experimental studies of equilibrium iron isotope fractionation in ferric aquo-chloro complexes. Geochim. Cosmochim. Acta 73, 2366–2381.
Hin, R.C., Schmidt, M.W., Bourdon, B., 2012. Experimental evidence for the absence of iron isotope fractionation between metal and silicate liquids at 1 GPa and 1250-1300C and its cosmochemical consequences. Geochim. Cosmochim. Acta 93, 164–181.
Jordan, M.K., Tang, H., Kohl, I.E., Young, E.D., 2019. Iron isotope constraints on planetesimal core formation in the early solar system. Geochim. Cosmochim. Acta 246, 461–477.
Karki, K., Stixrude, L., 2005. Structure and Freezing of $MgSiO_3$ liquid in Earth's lower mantle. Science 310, 297–299.
Kehm, K., Hauri, E.H., Alexander, C.O.D., Carlson, R.W., 2003. High precision iron isotope measurements of meteoritic material by cold plasma ICP-MS. Geochim. Cosmochim. Acta 67 (15), 2879–2891.
Lazar, C., Young, E.D., Manning, C.E., 2012. Experimental determination of equilibrium nickel isotope fractionation between metal and silicate from 500 C to 950 C. Geochim. Cosmochim. Acta 86, 276–295.
Liu, J., Dauphas, N., Roskosz, M., Hu, M.Y., Yang, H., Bi, W., Zhao, J., Alp, E.E., Hu, J.Y., Lin, J.F., 2017. Iron isotopic fractionation between silicate mantle and metallic core at high pressure. Nat. Commun. 8, 14377.
Luck, J.-M., Ben Othman, D., Albaréde, 2005. Zn and Cu isotopic variations in chondrites and iron meteorites: early solar nebula reservoirs and parent-body processes. Geochim. Cosmochim. Acta 69, 5351–5363.
Macris, C.A., Young, E.D., Manning, C.E., 2013. Experimental determination of equilibrium magnesium isotope fractionation between spinel, forsterite, and magnesite from 600 to 800 C. Geochim. Cosmochim. Acta 118, 18–32.
Mandernack, K.W., Bazylinski, D.A., Shanks, W.C., Bullen, T.D., 1999. Oxygen and iron isotope studies of magnetite produced by magnetotactic bacteria. Science 285 (5435), 1892–1896.
Murphy, C.A., Jackson, M, J.M., Sturhahn, W., 2013. Experimental constraints on the thermodynamics and sound velocities of hcp-Fe to core pressures. J. Geophys. Res. Solid Earth 118, 1999–2016.
Ni, P., Chabot, N.L., Ryan, C.J., Shahar, A., 2020. Heavy iron isotopes for iron meteorites caused by core crystallization. Nat. Geosci. https://doi.org/10.1038/s41561-020-0617-y. (In Press).
Northrop, D.A., Clayton, R.N., 1966. Oxygen-isotope fractionations in systems containing dolomite. The Journal of Geology 74 (2), 174–196.
Poitrasson, F., Halliday, A.N., Lee, D.C., Levasseur, S., Teutsch, N., 2004. Iron isotope differences between Earth, Moon, Mars and Vesta as possible records of contrasted accretion mechanisms. Earth Planet. Sci. Lett. 223, 253–266.
Poitrasson, F., Levasseur, S., Teutsch, N., 2005. Significance of iron isotope mineral fractionation in pallasites and iron meteorites for the core-mantle differentiation of terrestrial planets. Earth Planet. Sci. Lett. 234, 151–164.
Poitrasson, F., Roskosz, M., Corgne, A., 2009. No iron isotope fractionation between molten alloys and silicate melt to 2000C and 7.7 GPa: experimental evidence and implications for planetary differentiation and accretion. Earth Planet. Sci. Lett. 278, 376–385.
Poitrasson, F., Delpech, G., Grégoire, M., 2013. On the iron isotope heterogeneity of lithospheric mantle xenoliths: implications for mantle metasomatism, the origin of basalts and the iron isotope composition of the Earth. Contrib. Mineral. Petrol. https://doi.org/10.1007/s00410-013-0856-7.
Polyakov, V., 1998. On anharmonic and pressure corrections to the equilibrium isotopic constants for minerals. Geochim. Cosmochim. Acta 62, 3077–3085.
Polyakov, V., Clayton, R., Horita, J., Mineev, S., 2007. Equilibrium iron isotope fractionation factors of minerals: Reevaluation from the data of nuclear inelastic resonant X-ray scattering and Mössbauer spectroscopy. Geochim. Cosmochim. Acta 71, 3833–3846.
Polyakov, V.B., Mineev, S.D., 2000. The use of Mössbauer spectroscopy in stable isotope geochemistry. Geochim. Cosmochim. Acta 64 (5), 849–865.
Polyakov, V.I., 2009. Equilibrium iron isotope fractionation at core-mantle boundary conditions. Science 323, 912–914.

Roskosz, M., Sio, C.K., Dauphas, N., Bi, W., Tissot, F.L., Hu, M.Y., Zhao, J., Alp, E.E., 2015. Spinel–olivine–pyroxene equilibrium iron isotopic fractionation and applications to natural peridotites. Geochim. Cosmochim. Acta 169, 184–199.
Rubie, D.C., Jacobson, S.A., Morbidelli, A., O'Brien, D.P., Young, E.D., de Vries, J., Nimmo, F., Palme, H., Frost, D.J., 2015. Accretion and differentiation of the terrestrial planets with implications for the compositions of early-formed Solar System bodies and accretion of water. Icarus 248, 89–108.
Schauble, E. A., Rossman, G. R., and Taylor Jr, H. P. (2001). Theoretical estimates of equilibrium Fe-isotope fractionations from vibrational spectroscopy. Geochim. Cosmochim. Acta, 65 (15), 2487–2497.
Shahar, A., Young, E.D., Manning, C.E., 2008. Equilibrium high-temperature Fe isotope fractionation between fayalite and magnetite: an experimental calibration. Earth Planet. Sci. Lett. 268, 330–338.
Shahar, A., Ziegler, K., Young, E.D., Ricolleau, A., Schauble, E.A., Fei, Y., 2009. Experimentally determined Si isotope fractionation between silicate and Fe metal and implications for Earth's core formation. Earth Planet. Sci. Lett. 288 (1–2), 228–234.
Shahar, A., Mesa-Garcia, J., Kaufman, L.A., Hillgren, V.J., Horan, M.F., Mock, T.D., 2015. Sulfur-controlled iron isotope fractionation experiments of core formation in planetary bodies. Geochim. Cosmochim. Acta 150, 253–264.
Shahar, A., Schauble, E.A., Caracas, R., Gleason, A.E., Reagan, M.M., Xiao, Y., Shu, J., Mao, W., 2016. Pressure-dependent isotopic composition of iron alloys. Science 352 (6285), 580–582.
Shahar, A., Elardo, S.M., Macris, C.A., 2017. Equilibrium fractionation of non-traditional stable isotopes: an experimental perspective. Rev. Mineral. Geochem. 82 (1), 65–83.
Sio, C.K., Roskosz, M., Dauphas, N., Bennett, N.R., Mock, T., Shahar, A., 2018. The isotope effect for Mg-Fe interdiffusion in olivine and its dependence on crystal orientation, composition and temperature. Geochim. Cosmochim. Acta 239, 463–480.
Sossi, P.A., Foden, J.D., Halverson, G.P., 2012. Redox-controlled iron isotope fractionation during magmatic differentiation: an example from the Red Hill intrusion, S. Tasmania. Contrib. Mineral. Petrol. 164, 757–772.
Sossi, P.A., Nebel, O., Foden, J., 2016. Iron isotope systematics in planetary reservoirs. Earth Planet. Sci. Lett. 452, 295–308.
Sturhahn, W., Toellner, T., Alp, E.E., Zhang, X., Ando, M., Yoda, Y., Kikuta, S., Seto, M., Kimball, C.W., Dabrowski, B., 1995. Phonon density of states measured by inelastic nuclear resonant scattering. Phys. Rev. Lett. 74, 3832–3835.
Teng, F.-Z., Dauphas, N., Huang, S., Marty, B., 2013. Iron isotopic systematics of oceanic basalts. Geochim. Cosmochim. Acta 107, 12–26.
Trail, D., Savage, P.S., Moynier, F., 2019. Experimentally determined Si isotope fractionation between zircon and quartz. Geochim. Cosmochim. Acta 260, 257–274.
Weyer, S., Ionov, D., 2007. Partial melting and melt percolation in the mantle: the message from Fe isotopes. Earth Planet. Sci. Lett. 259, 119–133.
Weyer, S., Schwieters, J.B., 2003. High precision Fe isotope measurements with high mass resolution MC-ICPMS. Int. J. Mass Spectrom. 226 (3), 355–368.
Williams, H., McCammon, C.A., Peslier, A.H., Halliday, A.N., Teutsch, N., Levasseur, S., Burg, J.P., 2004. Iron isotope fractionation and the oxygen fugacity of the mantle. Science 304, 1656–1659.
Williams, H.M., Peslier, A., McCammon, C.A., Halliday, A.N., Levasseur, S., Teutsch, N., Burg, J.P., 2005. Systematic iron isotope variations in mantle rocks and minerals: the effects of partial melting and oxygen fugacity. Earth Planet. Sci. Lett. 235 (1–2), 435–452.
Williams, H.M., Wood, B.J., Wade, J., Frost, D.J., Tuff, J., 2012. Isotopic evidence for internal oxidation of the Earth's mantle during accretion. Earth Planet. Sci. Lett. 321-322, 54–63.
Young, E.D., Fogel, M.L., Rumble III, D., Hoering, T.C., 1998. Isotope-ratio-monitoring of O_2 for microanalysis of $^{18}O/^{16}O$ and $^{17}O/^{16}O$ in geological materials. Geochim. Cosmochim. Acta 62 (18), 3087–3094.
Zhu, X.K., Guo, Y., Williams, R.J.P., O'nions, R.K., Matthews, A., Belshaw, N.S., Canters, G.W., De Waal, E.C., Weser, U., Burgess, B.K., Salvato, B., 2002. Mass fractionation processes of transition metal isotopes. Earth Planet. Sci. Lett. 200 (1–2), 47–62.
Ziegler, K., Young, E.D., Schauble, E.A., Wasson, J.T., 2010. Metal–silicate silicon isotope fractionation in enstatite meteorites and constraints on Earth's core formation. Earth Planet. Sci. Lett. 295 (3–4), 487–496.